NMRlipids IV: Headgroup & glycerol backbone structures, and cation binding in bilayers with PE and PG lipids

Pavel Buslaev,[1] Fernando Favela-Rosales,[2] Patrick Fuchs,[3] Matti Javanainen,[4] Jesper J. Madsen,[5,6] Josef Melcr,[4,7] Markus S. Miettinen,[8] O. H. Samuli Ollila,[9,*] Chris G. Papadopoulos,[10] Antonio Peón,[11] Thomas J. Piggot,[12] and Pierre Poulain[3]

[1]*University of Jyväskylä*
[2]*Departamento de Investigación, Tecnológico Nacional de México, Campus Zacatecas Occidente, México*
[3]*Paris, France*
[4]*Institute of Organic Chemistry and Biochemistry of the Czech Academy of Sciences, Flemingovo nám. 542/2, CZ-16610 Prague 6, Czech Republic*
[5]*Department of Chemistry, The University of Chicago, Chicago, Illinois, United States of America*
[6]*Department of Global Health, College of Public Health, University of South Florida, Tampa, Florida, United States of America*
[7]*Groningen Biomolecular Sciences and Biotechnology Institute and The Zernike Institute for Advanced Materials, University of Groningen, 9747 AG Groningen, The Netherlands*
[8]*Department of Theory and Bio-Systems, Max Planck Institute of Colloids and Interfaces, 14424 Potsdam, Germany*
[9]*Institute of Biotechnology, University of Helsinki*
[10]*I2BC - University Paris Sud*
[11]*Spain*
[12]*Chemistry, University of Southampton, Highfield, Southampton SO17 1BJ, United Kingdom*

(Dated: May 20, 2020)

Abstract

INTRODUCTION

PE and PG lipids are most common lipids in bacteria [1]. Zwitterionic PE is the second most abundant glycerophospholipid in eukaryotic cells and has been related to the diseases [2–4]. Anionic PG lipids are less abundant, but is also proposed to be fundamental for terrestrial life [5]. PE and PG affect membrane protein functionality [6] and bind to various proteins [7]. PE headgroup is also prone for negative membrane curvature and causes membrane fusion [3, 8]. Therefore, the PE and PG headgroup structures play probably essential roles in many biological processes.

Structural details of lipid headgroups are mainly studied using NMR experiments, which suggest that the glycerol backbone structures are largely similar irrespectively of the headroup [9], glycerol backbone and headgroup structure and behaviour are similar in model membranes and in bacteria [9–11], and the headgroup structures are similar in PC, PE and PG lipids, while headgroup is more rigid in PS lipids [12, 13]. Some attempts to resolve conformational ensembles from NMR for PC and PE lipids have been made, but lesser extend for PG or PS lipids [14–16]. Classical molecular dynamics simulations could potentially give such ensembles and therefore enable the detailed studies of lipid headgroup behaviour in complex biomolecular systems, but current force fields are not accurate enough to reproduce the correct conformational ensembles for PC and PS headgroups [17, 18]. Several MD simulations of PE and PG lipids have been published especially in the context of modeling inner membrane of Gram-negative bacteria [19–31] **1.There may be some relevant publication missing from here**, but evaluation of glycerol backbone and headgroup structures against experiments is rare [25].

Besides the structure, also ion binding may regulate biophysical activity of especially negatively charged lipid headgroups [11]. Monovalent cation (except Lithium) binding to zwitterionic PC and anionic PS headgroups is very weak, while multivalent ion binding is stronger but still weak [18, 32–35]. The ion binding affinity data for PE is more scarce [36], but large differences to PC would be surprising. Negatively charged lipids are suggested to bear same cation binding constants than zwitterionic lipids, but the amount of bound ions to negatively charged membranes would still be larger because the concentration of cations in the vicinity of membranes would be higher [11]. On the other hand, anionic PS lipids are proposed chelate with calcium ions [37–39]. In simulations, the cation binding affinity to PC and PS membranes is typically overestimated [18, 35], which can be improved by applying the ECC to the partial charges of the force fields [40, 41].

Here, we use open collaboration and order parameters of glycerol backbone and headgroup to evaluate the accuracy of PE and PG heagroup structures, and the cation binding affinity to anionic membranes containing PG lipids in the current MD simulation force fields. The force field giving the best description for glycerol backbone and headgroup structures of PC, PS, PG and PE headgroups (CHARMM36) reproduces the essential differences in order parameters between these headgroups, and therefore enables the analysis of structural differences between the headgroups.

METHODS

Experimental C–H bond order parameters

The headgroup and glycerol backbone C–H bond order parameter magnitudes and signs of POPE and POPG were determined by measuring the chemical-shift resolved dipolar splittings with a R-type Proton Detected Local Field (R-PDLF) experiment [42] and S-DROSS experiments [43] using natural abundance ^{13}C solid state NMR spectroscopy as described previously [44, 45]. POPE and POPG powder were purchased from Avanti polar lipids. The NMR experiments were identical to our previous work [18]. **2.Is this enough and correct, or should we repeat some methods from the NMRlipidsIVps paper?** The POPE experiments were recorded at 310 K and POPG experiments at 298 K, where the bilayers are in the liquid disordered phase [46].

Molecular dynamics simulations

Molecular dynamics simulation data were collected using the Open Collaboration method [17], with the NMRlipids Project blog (`nmrlipids.blogspot.fi`) and GitHub repository (`github.com/NMRlipids/NMRlipidsIVotherHGs`) as the communication platforms. The simulated systems of pure PE and PG bilayers without additional ions are listed in Tables I and II, and lipid mixtures with additional ions in Table III. Further simulation details are given in the SI, and the simulation data are indexed in a searchable database available at `www.nmrlipids.fi`, and in the NMRlipids/MATCH repository (`github.com/NMRlipids/MATCH`).

The C–H bond order parameters were calculated directly from the carbon and hydrogen positions using the definition

$$S_{\mathrm{CH}} = \frac{1}{2}\langle 3\cos^2\theta - 1\rangle, \qquad (1)$$

where θ is the angle between the C–H bond and the membrane normal (taken to align with z, with bilayer periodicity in the xy-plane). Angular brackets denote average over all sampled configurations. The order parameters were first calculated averaging over time separately for each lipid in the system. The average and the standard error of the mean were then calculated over different lipids. Python programs that use the MDAnalysis library [47, 48] used for all atom simulations is available in Ref. 49 (`scripts/calcOrderParameters.py`). For united atom simulations, the trajectories with hydrogens having ideal geometry were constructed first using either buildH program [50] or (`scratch/opAAUA_prod.py`) in Ref. 49, and the order parameters were then calculated from these trajectories. This approach has been tested against trajectories with explicit hydrogens and the deviations in order parameters are small [50, 51].

3.BuildH program is now cited with a direct link to the GitHub repo. I think that a release to Zenodo would be nice in the final publication.

4.Maybe we should also shortly discuss here about the reasons for slight dependence of order parameter values on the method used to reconstruct hydrogens?

The ion number density profiles were calculated using the `gmx density` tool of the Gromacs sofware package [52].

TABLE I: List of MD simulations with PE lipids.

lipid/counter-ions	force field for lipids / ions	NaCl (M)	[a]N_l	[b]N_w	[c]N_c	[d]T (K)	[e]t_{sim}(ns)	[f]t_{anal} (ns)	[g]files
POPE	CHARMM36 [**?**]	0	144	5760	0	310	500	400	[53]
POPE	CHARMM36 [**?**]	0	500	25000	0	310	500	100	[54]
POPE	CHARMM36 [**?**]	0.11	500	25000	50	310	500	100	[55]
POPE	CHARMM36ua [**?**]	0	336	15254	0	310	2×200	2×100	[56]
DPPE	Slipids [57]	0	288	9386	0	336	200	100	[58]
POPE	Slipids [57**?**]	0	336	?	0	310	2×200	2×100	[59]
POPE	Slipids [**?**]	0	500	25000	0	310	500	100	[60]
POPE	Slipids [**?**] 5.	0.11	500	25000	50	310	500	100	[61]
DPPE	GROMOS-CKP [**?**]	0	128	3655	0	342	2×500	2×400	[62]
POPE	GROMOS-CKP [**?**]	0	128	3552	0	313	2×500	2×400	[63]
POPE	GROMOS-CKP [**?**]	0	500	25000	0	310	500	100	[64]
POPE	GROMOS-CKP [**?**]	0.11	500	25000	50	310	500	100	[65]
DOPE	GROMOS-CKP [**?**]	0	128	4789	0	271	2×500	2×400	[66]
POPE	GROMOS 43A1-S3 [**?**]	0	128	3552	0	313	2×200	2×100	[67]
POPE	OPLS-UA vdW on H [**?**]	0	128	3328	0	303	2×200	2×100	[68]
POPE	OPLS-UA [**?**]	0	128	3328	0	303	2×200	2×100	[69]
POPE	OPLS-MacRog [70]	0	144	5760	0	310	500	350	[71]
POPE	Berger-Vries [**?**]	0	128	3552	0	303	2×200	2×100	[72]
POPE	Berger-largeH [**?**]	0	128	3552	0	303	2×200	2×100	[73]
DOPE	Berger-Vries [**?**]	0	128	4789	0	271	2×200	2×100	[74]
DOPE	Berger-largeH [**?**]	0	128	4789	0	271	2×300	2×100	[75]
POPE	LIPID17 [**?**]	0	500	25000	50	310	500	100	[76]
POPE	LIPID17 [**?**]	0.11	500	25000	50	310	500	100	[77]

[a]Number of lipid molecules with largest mole fraction
[b]Number of water molecules
[c]Number of additional cations
[d]Simulation temperature
[e]Total simulation time
[f]Time used for analysis
[g]Reference for simulation files

6.We need citations for the force fields.

TABLE II: List of MD simulations with PG lipids.

lipid/counter-ions	force field for lipids / ions	NaCl (M)	[a]N_l	[b]N_w	[c]N_c	[d]T (K)	[e]t_{sim}(ns)	[f]t_{anal} (ns)	[g]files
POPG/K^+	CHARMM36 [**?**] 7.	0	118	4110	0	298	100	100	[78]
POPG	CHARMM36 [**?**]	0.11	500	25000	49	310	500	100	[79]
POPG	CHARMM36 [**?**]	0	500	25000	0	310	500	100	[80]
POPG/Na^+	Slipids [81]	0	288	10664	0	298	250	100	[82]
DPPG/Na^+	Slipids [81]	0	288	11232	0	314	200	100	[83]
DPPG/Na^+	Slipids [81]	0	288	11232	0	298	400	100	[84]
POPG	Slipids [**?**] 8.	0	500	25000	0	310	500	100	[85]
POPG	Slipids [**?**] 9.	0.11	500	25000	49	310	500	100	[86]
POPG	LIPID17 [**?**]	0	500	25000	0	310	500	100	[87]
POPG	LIPID17 [**?**]	0.11	500	25000	49	310	500	100	[88]
POPG	GROMOS-CKP [**?**]	0	500	25000	0	310	500	100	[89]
POPG	GROMOS-CKP [**?**]	0.11	500	25000	49	310	500	100	[90]

[a]Number of lipid molecules with largest mole fraction
[b]Number of water molecules
[c]Number of additional cations
[d]Simulation temperature
[e]Total simulation time
[f]Time used for analysis
[g]Reference for simulation files

10.We need citations for the force fields.

TABLE III: List of MD simulations with PE and PG lipids mixed with PC.

lipid/counter-ions	force field for lipids / ions	NaCl (M)	$CaCl_2$ (M)	[a]N_l	[b]N_w	[c]N_c	[d]T (K)	[e]t_{sim}(ns)	[f]t_{anal} (ns)	[g]files
POPC	CHARMM36 [**?**]	0.11	0	500	25000	48	310	500	100	[91]
POPC:POPG (7:3)	CHARMM36 [**?**]	0.11	0	350	?	?	310	500	100	[92]
POPC:POPG (1:1)/K^+	CHARMM36 [**?**]	0	0	250:250	18158	0	298	200	200	[93]
POPC:POPG (1:1)	CHARMM36 [**?**]	0	0.34 **11.**	250:250	20798	128	298	200	200	[94]
POPC:POPG (1:1)	CHARMM36 [**?**]	0	1.36 **12.**	250:250	18114	445	298	200	200	[95]
POPC:POPG (4:1)/K^+	CHARMM36 [**?**]	0	0	400:100	18664	0	298	200	200	[96]
POPC:POPG (4:1)/K^+	CHARMM36 [**?**]	0	1.0 **13.**	400:100	18647	419	298	200	200	[97]
POPC	CHARMM36 [**?**]	0	0	256	8704	0	300	300	250	[98]
POPC:POPE (1:1)	CHARMM36 [**?**]	0	0	128	8704	0	300	300	250	[99]
POPC	Slipid / ?? [57**?**]	0.11	0	500	25000	48	310	500	100	[100]
POPC:POPG (7:3)	Slipid / Dang [57**? ? ?**]	0	0	350:150	25000	0	310	500	100	[101]
POPC:POPG (1:1)	Slipid / Dang [57**? ? ?**]	0	0	128:128	12800	0	298	500	400	[102]
POPC:POPG (1:1)	Slipid / Dang [57**? ? ?**]	0	0.1	128:128	12800	23	298	500	400	[102]
POPC:POPG (1:1)	Slipid / Dang [57**? ? ?**]	0	0.2	128:128	12800	46	298	1500	500	[102]
POPC:POPG (1:1)	Slipid / Dang [57**? ? ?**]	0	0.5	128:128	12800	115	298	1500	500	[102]
POPC:POPG (1:1)	Slipid / Dang [57**? ? ?**]	0	1.0	128:128	12800	230	298	1500	500	[102]
POPC:POPG (4:1)	Lipid17 / Dang [**? ? ?**]	0	0	350:88	26265	0	298	400	350	[**?**]
POPC:POPG (4:1)	Lipid17 / Dang [**? ? ?**]	0	0.1	350:88	26124	47	298	400	150	[**?**]
POPC:POPG (4:1)	Lipid17 / Dang [**? ? ?**]	0	1.0	350:88	24840	475	298	1200	200	[**?**]
POPC:POPG (1:1)	Lipid17 / Dang [**? ? ?**]	0	0	150:150	31572	0	298	320	200	[103]
POPC:POPG (1:1)	Lipid17 / Dang [**? ? ?**]	0	0.1	150:150	31401	57	298	720	198	[**?**]
POPC:POPG (1:1)	Lipid17 / Dang [**? ? ?**]	0	1.0	150:150	29865	569	298	720	200	[**?**]
POPC	Berger [**?**] **14.**	0	0	256	10240	0	300	300	200	[104]
POPC:POPE (1:1)	Berger [**?**] **15.**	0	0	128	11008	0	300	300	200	[105]
POPC:DOPE (1:1)	Berger [**?**] **16.**	0	0	128	10240	0	300	300	200	[106]
DOPC	Berger [**?**] **17.**	0	0	256	11008	0	300	300	200	[107]
DOPC:DOPE (1:1)	Berger [**?**] **18.**	0	0	128	11008	0	300	300	200	[108]

[a]Number of lipid molecules with largest mole fraction
[b]Number of water molecules
[c]Number of additional cations
[d]Simulation temperature
[e]Total simulation time
[f]Time used for analysis
[g]Reference for simulation files

19.Data for POPC:POPG mixtures by listed by Antonio Peon is missing from this table

20.We need citations for the force fields.

RESULTS AND DISCUSSION

Headgroup and glycerol backbone order parameters of POPE and POPG from ^{13}C NMR

Absolute values of the headgroup and glycerol backbone order parameters from PE and PG lipids are measured previously using ^{2}H NMR [9, 12, 109, 110]. Because also the order parameter signs bear essential information about the lipid structures [17, 111], we measured the magnitudes and signs of POPE and POPG C–H bond headgroup and glycerol backbone order parameter in liquid phase using the 2D-RPDLF and S-DROSS experiments, as described previously [18, 44, 45]. For POPE, the glycerol backbone and α-carbon peaks in INEPT spectra were assigned based on previously measured POPC spectra [44] and the β-carbon peak was assigned based on ^{13}C chemical shift table for amines available at `https://www.chem.wisc.edu/areas/reich/nmr/c13-data/cdata.htm` (Fig. S1). For POPG, the glycerol backbone peaks in INEPT spectra were assigned based on previously measured POPC spectra [44], while α and γ-carbon peaks **21.How were these assigned?** (Fig. S2). The numerical value of the β-carbon order parameter could not be determined, because its peak overlapped with the g_2 peak from glycerol backbone in POPG. However, the order parameter of β-carbon is expected to be clearly smaller than for g_2 based on previous ^{2}H NMR measurements [9, 12, 110]. Therefore, the beginning of the S-DROSS curve gives the sign for g_2 order parameter and end for β (Fig. S2 (E)). This is confirmed with SIMPSON calculations using negative value for g_2 and positive value for β order parameter (Fig. S3). **22.Details to be checked by Tiago.**

As discussed previously for PC and PS headgroups [18, 111], also the headgroup and glycerol backbone order parameters of PE and PG are essentially independent of acyl chain composition, and therefore manifest mainly headgroup chemistry (Fig. 1). The glycerol backbone order parameters are similar for all the lipids, although they move slightly toward positive values (closer to zero) in the order PC $<$ PE $<$ PS $<$ PG. Also the headgroup order parameters of PC lipids are close PE, althought the latter gives systematically slightly more positive values (Fig. 1). The α-carbon order parameter of PG is similar to PE and PG, while the positive value of β-carbon is distinct from the other lipids. Notably, this difference was not observed in previous ^{2}H NMR experiments, because absolute value of β-carbon order parameter is similar in PG, PE and PC lipids and the order parameter signs were not measured [9, 12, 110].

In conclusion, the order parameter experiments suggest that the glycerol backbone conformations in all lipids and the headgroup conformations in PC and PE lipids are relatively similar, while PS and PG headgropus exhibit distinct conformational sampling. The details of sampled conformation are difficult to deduce from order parameters only, but the distinct headgroup order parameters of PS lipids are previously related to the more rigid structure of the headgroup [13, 18, 112].

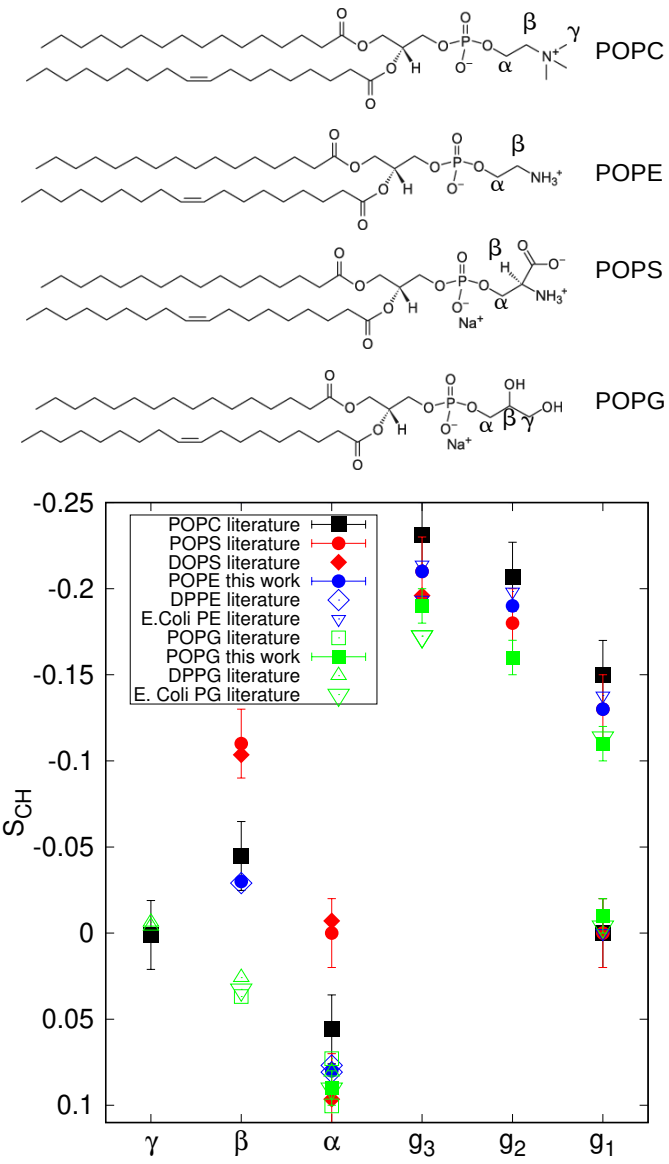

FIG. 1: (top) Chemical structure of different lipids. (bottom) Headgroup and glycerol backbone order parameters from different experiments in lamellar liquid disordered phase. The values and signs for POPE (310 K) and POPG (298 K) measured in this work, and for POPS (298 K) [18] and POPC (300 K) [44, 45] previously using ^{13}C NMR. The literature values for DOPS with 0.1M of NaCl (303 K) [112], POPG with 10nM PIPES (298 K) [110], DPPG with 10mM PIPES and 100mM NaCl (314 K) [12], DPPE (341 K) [109], E.coliPE and E.coliPG (310 K) [9] are measured using ^{2}H NMR. The signs from ^{13}C NMR are used also for the literature values.

23.The bottom figure could be clarified as Fig. 2 in the NMRlipids IVps paper.

Headgroup and glycerol backbone of POPE and POPG in MD simulations

Headgroup and glycerol backbone order parameters of PE and PG lipids show wide variation between different force fields and none of the force fields reproduce all values within experimental error bars. (Figs. 2 and 3), as observed previously also for PC and PS lipids [17, 18]. The poor performance of headgroup order parameters in Berger model can be probably explained by ring like structures seen in Fig. 6 in Ref. 113, which is a typical feature for Berger based lipid force fields containing explicit hydrogen atoms in the head group [24, 25, 114]. The poor performance of glycerol backbone of Slipids simulations is systemically observed also for other lipids in previous studies [17, 18]. **24.Should we comment more the relative quality of different force fields and/or make the subjective force field ranking figures? https://github.com/NMRLipids/NMRlipidsIVPEandPG/issues/8**

Without further discussion about poorly performing force fields, we focus on more detailed analysis of CHARMM36 simulations, which captures the essential differences between PC, PS, PG and PE headroup order parameters (Fig. 4) with the exception of β-carbon order parameter of PC which is too negative when compared with PS or PE order parameter, or with experiments [17]. Characteristic dihedral conformations in PS headgroup are asymmetric conformations preferring gauche 270° conformations in N-C_β-C_α-O_α and C_β-C_α-O_α-P dihedrals. In PG headgroup, the O_β-C_β-C_α-O_α dihedral (corresponding N-C_β-C_α-O_α dihedral in other lipids) is mostly in trans conformation, and C_β-C_α-O_α-P has asymmetric tendency to be in gauche 60° conformation. Main difference between PC and PE is the lower probability of trans state in C_β-C_α-O_α-P PC dihedral, which could be a potential reason for the too negative β headgroup order parameter in PC.

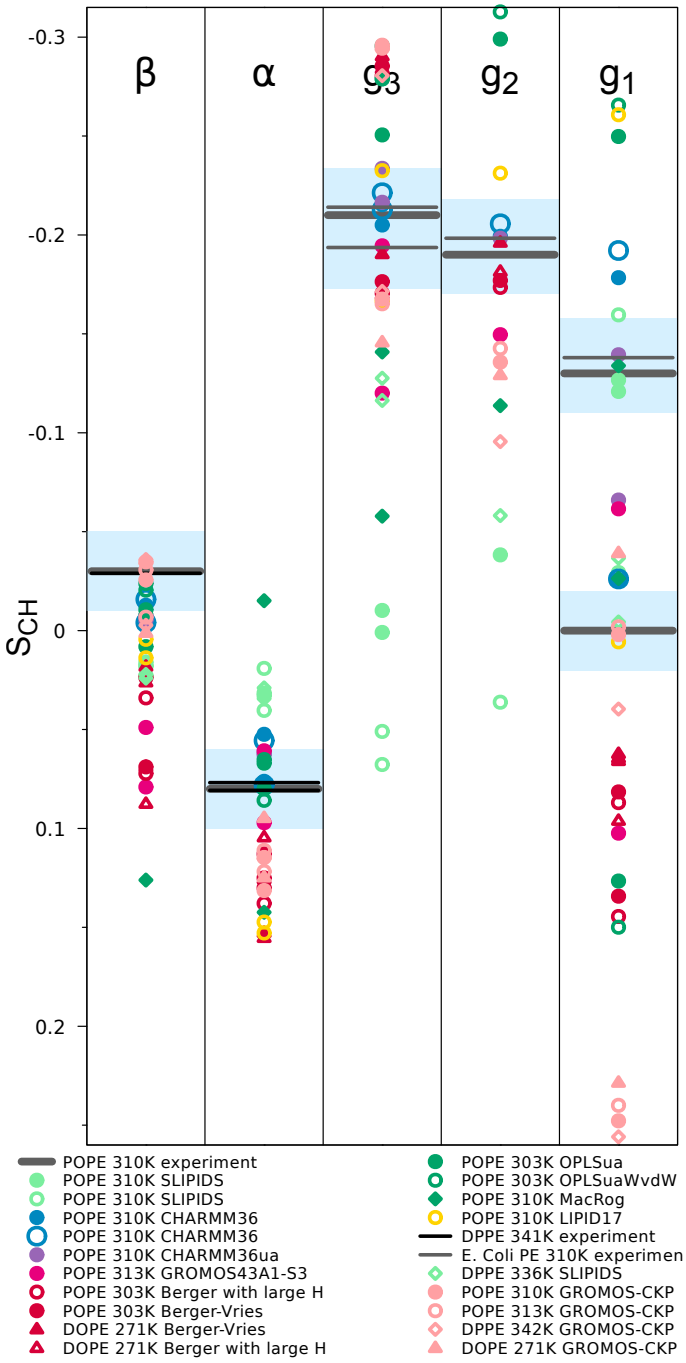

FIG. 2: The headgroup and glycerol backbone order parameters of PE lipids from experiments (POPE and signs this work, DPPE from Ref. 109 and E.coliPE from Ref. 9) and simulations with different force fields.

25.This should be clarified as in NMRlipidsI and error bars should be added. Probably larger error bars for united atom models based on the report by Fuchs et al.

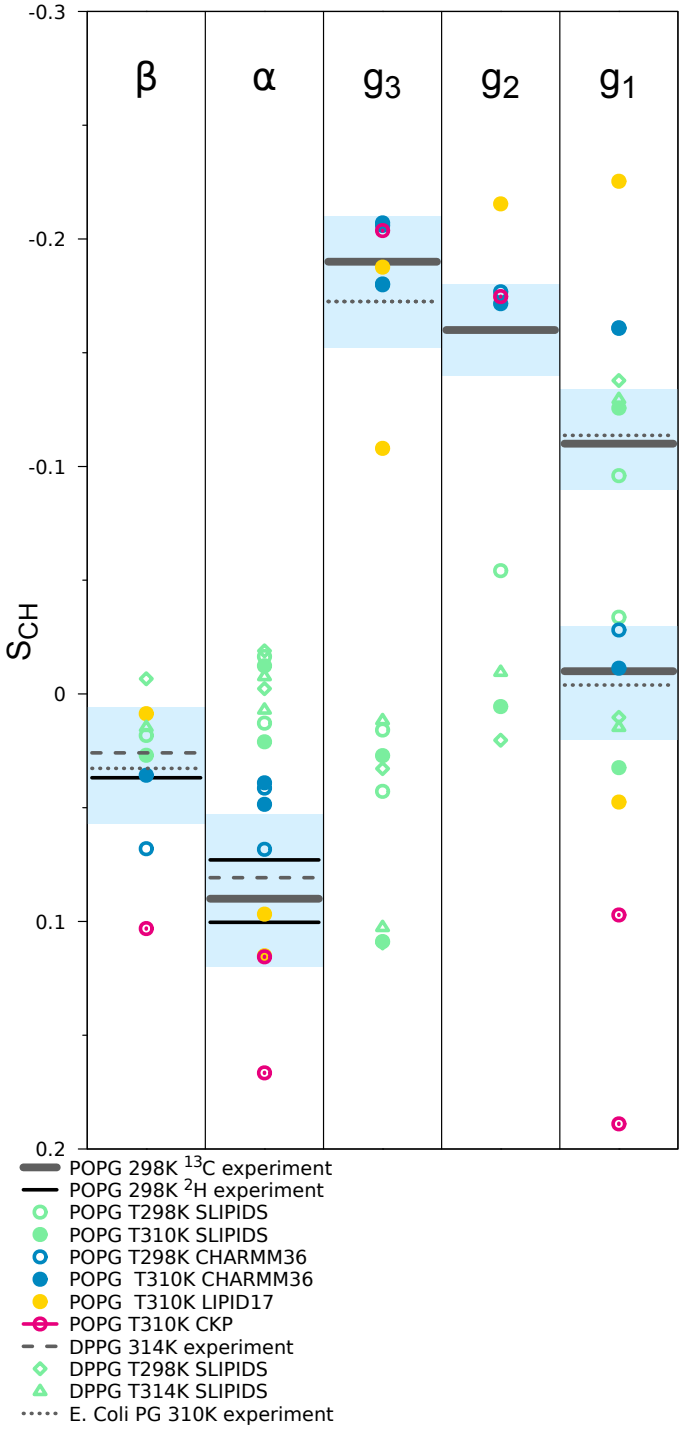

FIG. 3: The headgroup and glycerol backbone order parameters of PG lipids from experiments (POPG and signs from this work and from Ref. 110, DPPG with 100mM NaCl from Ref. 12,and E.Coli PG results from Ref. 9). and simulations with different force fields.

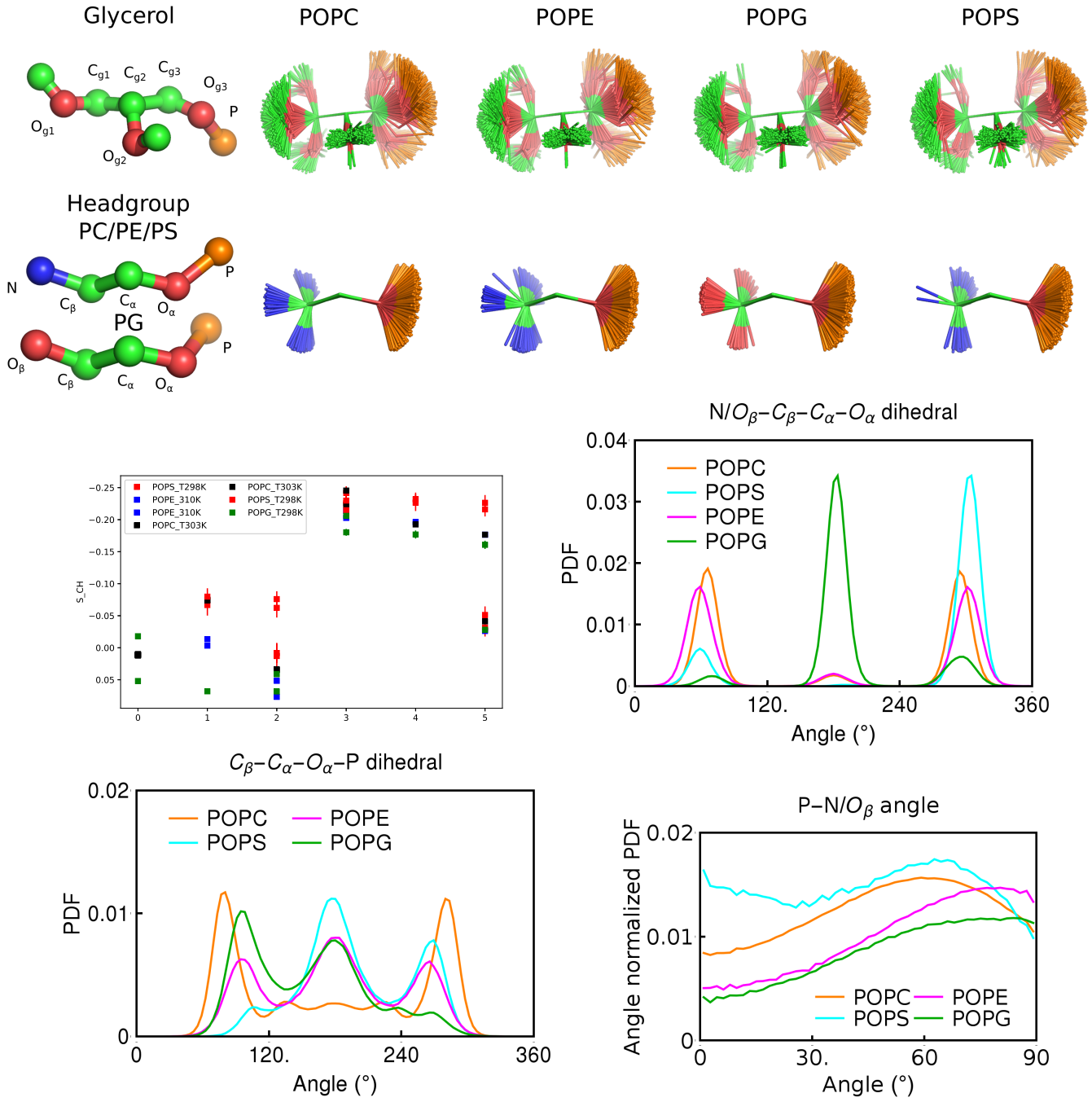

FIG. 4: Overlayed snapshots and dihedral angle distributions from CHARMM36 simulations of different lipids which give the best agreement with experiments.

26.The differences observed in dihedral distributions are not visible in the snapshot figures.

27.Why integral of the P-N angle distributions are not the same?

28.More detailed discussion of this figure is in https://github.com/NMRLipids/NMRlipidsIVPEandPG/issues/9

PC headgroup interactions with PE and PG

In experiments, the PC headgroup order parameters increase with the addition of negatively charged PG or PS lipids, but are not affected by the addition of zwitterionic PE and SM lipids or cholesterol (Fig. 5). This can be explained by the electrometer concept, which suggests that the headgroup dipole tilts more parallel to the membrane plane upon addition of negative charge to the membrane [10, 116, 117]. The response of PC headgroup order parameters to PE by the tested CHARMM36 and Berger-OPLS force fields, although CHARMM36 slightly overestimates the changes (Fig. 5). The good performance of Berger-OPLS simulations is notable because the response of headgroup order parameters to cholesterol was significantly overestimated by the Berger/Hltje force field in our previous work [17]. **29.This is text by P. Fuchs, copied from the blog.**

Area results in nm^2, the error is $<=$ 0.003 nm^2

- pure POPC

CHARMM36: 0.624

Berger : 0.649

- POPC/POPE 50:50

CHARMM36 : POPC 0.609, POPE 0.557

Berger-hacked: POPC 0.637, POPE 0.632

—

One can see that CHARMM 36 predicts a drop in the area on going from pure POPC to POPC/POPE 50:50. This means that POPC pack tightly to POPE. In contrast, the values for Berger are not that changed. The POPE value predicted by CHARMM 36 (in the mixture POPC/POPE 50:50) is much smaller than that predicted by Berger.

——-

The experimental acyl chain order parameters for POPE [118] seem larger than reported for POPC [44], which supports the more condensed PE bilayer. This is interesting, but not exactly the core message of the manuscript. Maybe we should mention this very briefly? For example, we could just report the areas per lipid (without distinguishing PC and PE) and mention the difference between CHARMM36 and Berger. I have opened an issue for this: https://github.com/NMRLipids/NMRlipidsIVPEandPG/issues/7

None of the force fields fully reproduces the PC headgroup order parameter response to the increasing amount of PG, which may be related to the counterion binding affinity (see also the next section) [18]. In all force fields except Slipids, the order parameters of different hydrogens attached to the α-carbon are responsing differently when mixed with PE or PG lipids **30.Maybe we should figure out what is the reason for this?**

Maybe we should analyze the P-N vector angle from different simulations?

https://github.com/NMRLipids/NMRlipidsIVPEandPG/issues/10.

For β-carbon order parameter in PG headgroup, experiments report mild increase [115] or no change [110] upon addition of PC lipids (Fig. 6). Simulations with all the tested force fields give only very small changes also for the α-carbon order parameter (Figs. S4 and 6). Therefore, the simulations are generally in line with experiments, suggesting that the interactions with PC do not essentially effect the PG headgroup structure. This suggests that the interactions between PG and PC headgroups are captured better in simulations than for PS headgroup, where all the force fieds significantly overestimated the structural response of PS headgroup to the interactions with PC lipids [117].

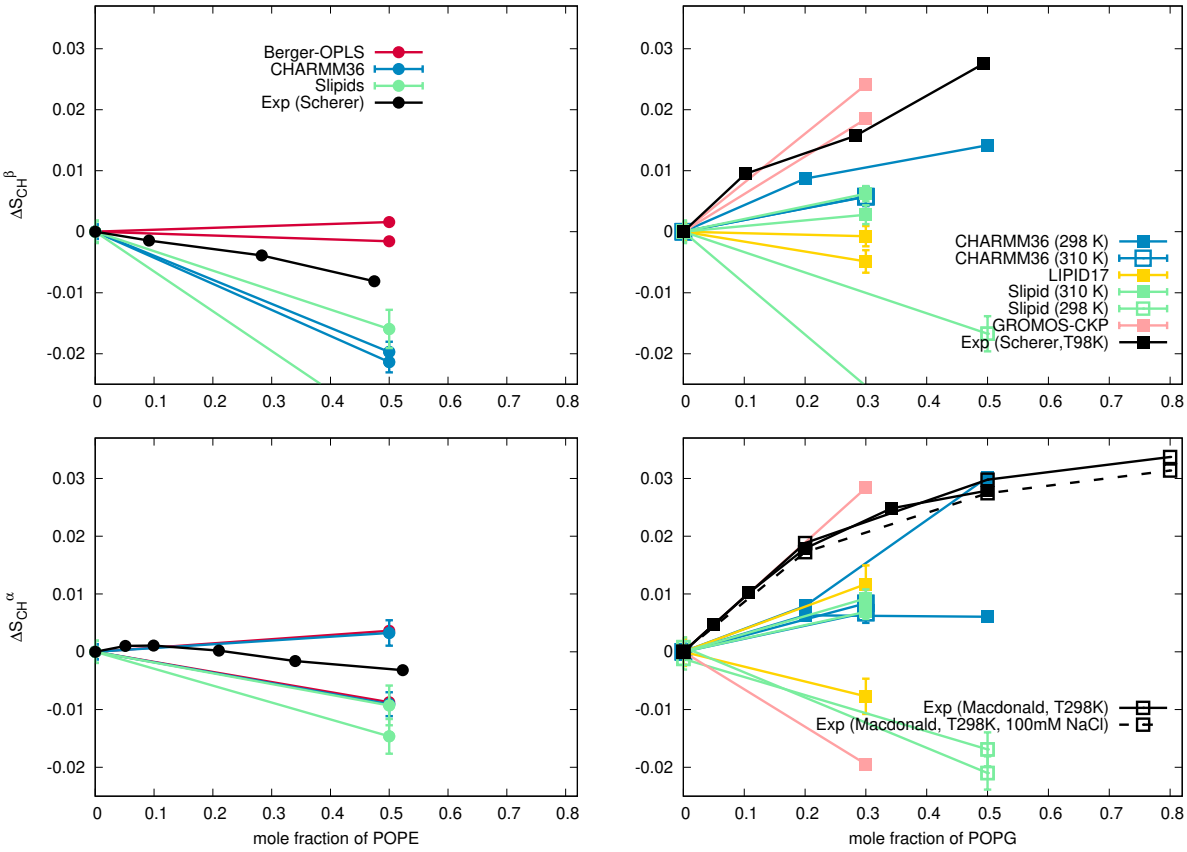

FIG. 5: Modulation of POPC headgroup order parameters with increasing amount of POPE (left) and POPG (right) in bilayer from experiments [10, 115] and simulations with different force fields. Signs are determined as discussed in [17, 111].

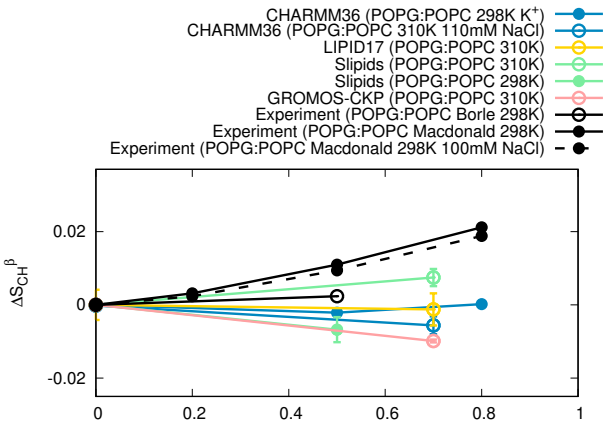

FIG. 6: Modulation of PG lipid headgroup order parameters with the increasing amount of PC in lipid bilayer from experiments [110, 115] and simulations with different force fields.

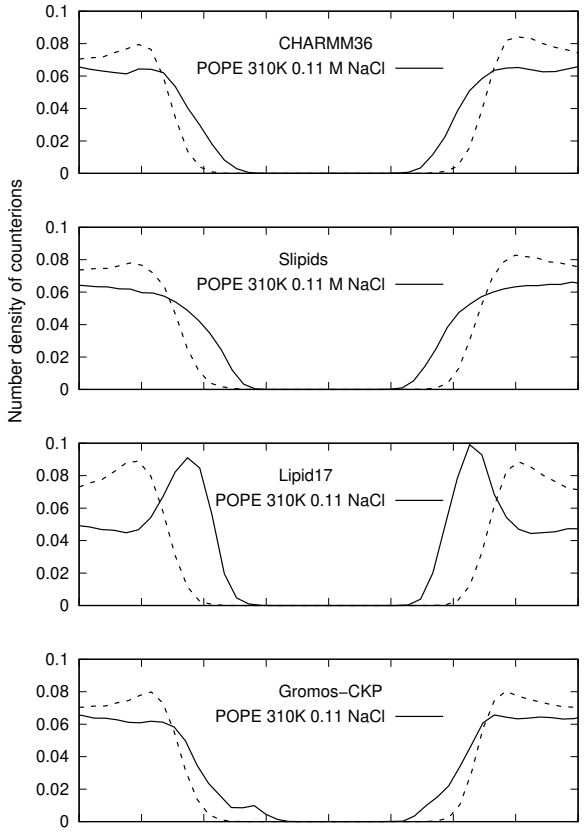

FIG. 7: Sodium (solid line) and choride ion density profiles along membrane normal from different simulations with PE lipids.

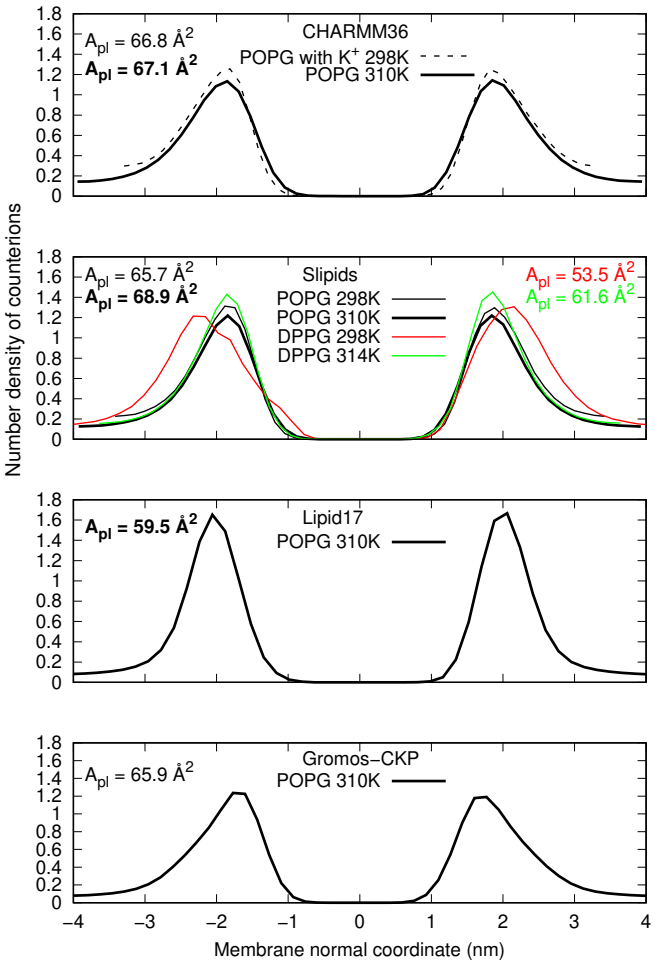

FIG. 8: Counterion densities and area per lipids from simulations with PG lipids. Experimental area for POPG at 303 K is 66.1 Å^2 and 67 Å^2 for DPPC at 323 K [119].

Sodium binding to PE and PG lipid bilayers

Sodium binding affinity to PE lipids has not been measured experimentally, but large differences to PC would be surprising. The sodium binding affinity to POPE depends on the used force field (Fig. 7), but lesser extend than reported previously for PC [35]. Because some simulation and ion parameters are not identical with the previous work [35] **31.This should be finished once we have the simulation details**, we compare POPE results to the POPC simulations ran with identical parameters (Fig. S5). In Lipid17 with the strongest sodium binding affinity to POPE, the binding affinity is approximately similar to POPC. Slipids and CHARMM36 exhibit slightly, and GROMOS-CKP substantially weaker binding to POPE than to POPC. Assuming that the binding to POPE would be similar than to POPC, the sodium binding affinity to POPE is potentially realistic in CHARMM36, Slipids, and GROMOS-CKP simulations here, but substantially overestimated in Lipid17 simulation.

Simulations with PG lipids give similar dependence on force field as observed in POPE simulations: Lipid 17 simulations exhibits stronger counter-ion binding affinity to pure POPG bilayer than CHARMM36, Slipids, and GROMOS-CKP simulations, which are roughly similar (Fig. 8). Lipid17 also exhibits less increase in POPC headgroup order parameters upon addition of POPG than other simulations (Fig. 5), and lower area per molecule (59.5 Å^2) than in experiments (66.1 Å^2). In our previous study about PS lipids [117], such behaviour was related to the overestimated counterions binding and shielding the electrostatic repulsion between PG headgroups in bilayers.Even though the area per lipid in CHARMM36, Slipids, and GROMOS-CKP simulations is in good agreement with experiments (Fig. 8), the experimental increase in POPC headgroup order parameters upon addition of POPG are not fully reproduced (Fig. 5). Therefore we conclude that the counter-ion binding affinity is overestimated in Lipid17 simulations, while the other simulations are more realistic, but slight overbinding cannot be excluded.

Calcium binding to PE and PG lipid bilayers

To evaluate the calcium binding in simulations of lipid bilayers containing PG lipids, we calculated the changes in headgroup order parameters of POPC:POPG (1:1) and (4:1) mixtures upon addition of $CaCl_2$, and compared these with the available experimental data [110, 115]. The headgroup order parameters of PC lipids can be used to measure the ion binding affinity to lipid bilayers because their magnitude is linearly proportional to the amount of bound charge in bilayer [35, 116]. This molecular electrometer concept can be used also for bilayers containing PC lipids mixed with charged lipids [18, 34, 110, 115]. The headgroup order parameters can be used to evaluate MD simulations against experimental data, because they can be directly calculated from MD simulations [35].

The decrease of POPC headgroup order parameters in mixtures with POPG lipids with increasing $CaCl_2$ concentration is overestimated in Slipids and Lipid17 simulations (Figs. 9 and S6) indicating too strong binding affinity of calcium into the bilayers as previously observed for pure PC lipid bilayers and mixtures with PS lipids [18, 35]. **33.CHARMM results to be mentioned once we have the new simulations.** The calcium binding affinity to lipid bilayers with PC and PS lipids was recently improved by applying the electronic continuum correction (ECC) to Amber Lipid14/17 force fields [40**?**]. In this approach, the electronic polarizability is implicitly included in the classical force fields by scaling the charges with constant factors [**?**]. Here, we make a ECC-POPG force field by applying the scaling factors originally used for POPS also to POPG, i.e., we multiply charges and Lennard-Jones σs of headgroup, glycerol backbone, and carbonyl regions with f_q=0.75 and f_σ=0.89, respectively [**?**]. ECC-POPG model gives a weaker calcium binding affinity (Fig.10) and better agreement with the experimental PC headgroup order parameter changes (Fig. 9) for POPC:POPG mixtures than the original Lipid17 model **34.to be finished when we have all the data**, indicating that the ECC improves the simulation predictions of calcium binding affinity as previously observed for PC and PS lipids [40**?**].

Experimental data for the β-carbon order parameter of POPG shows a rapid decrease with increasing $CaCl_2$ concentrations up to 10 mM and more modest decrease with larger concentrations (Fig. 9) [110]. This behaviour is similar to that of β-carbon order parameters of POPC, but essentially different than observed for POPS, where β-carbon order parameters increases with addition of calcium [18]. Experimentally measured changes of PG α-carbon order parameters upon addition of calcium are not available. Lipid17 and Slipids force fields correctly capture the PG β-carbon order parameter response to $CaCl_2$ even thought the binding affinity was too large based on the comparison of PC headgroup order parameter changes with experiments. While applying ECC to Lipid17 improved the PC headgroup order parameter response and binding affinity, the response of PG β-carbon order parameter to calcium is too weak in this model. The response of PG α-carbon order parameters to $CaCl_2$ differs between force fields, but experimental data to evaluate these predictions is not available.

35.To be finished once we have the new CHARMM simulations and conformational changes of PG analyzed.

36.We still need more data to finish the discussion. More detailed discussion is in https://github.com/NMRLipids/NMRlipidsIVPEandPG/issues/12

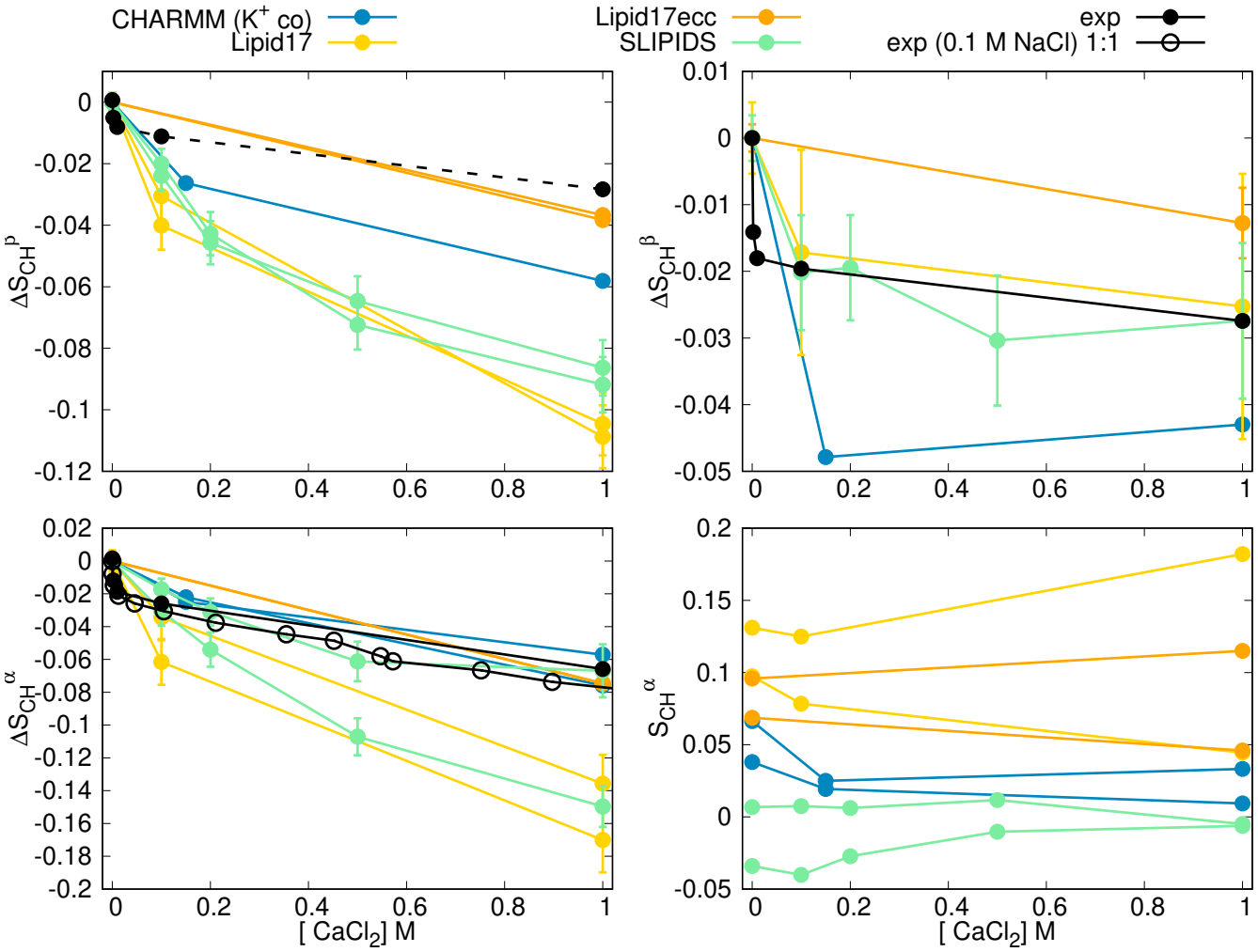

FIG. 9: Modulation of headgroup order parameters of POPC (*left*) and POPG (*right*) in POPC:POPG (1:1) mixture upon addition of $CaCl_2$ in 298 K temperature from experiments [110, 115] and simulations. The β-carbon order parameter of POPC (dashed line on top left) is not directly measured but calculated from empirical relation $\Delta S_\beta = 0.43\Delta S_\alpha$ [120]. The changes with respect to the systems without $CaCl_2$ are shown for other data than for the α-carbon of POPG for which experimental order parameter is not available.

32.CHARMM36 simulations should be longer and with Na couterions.

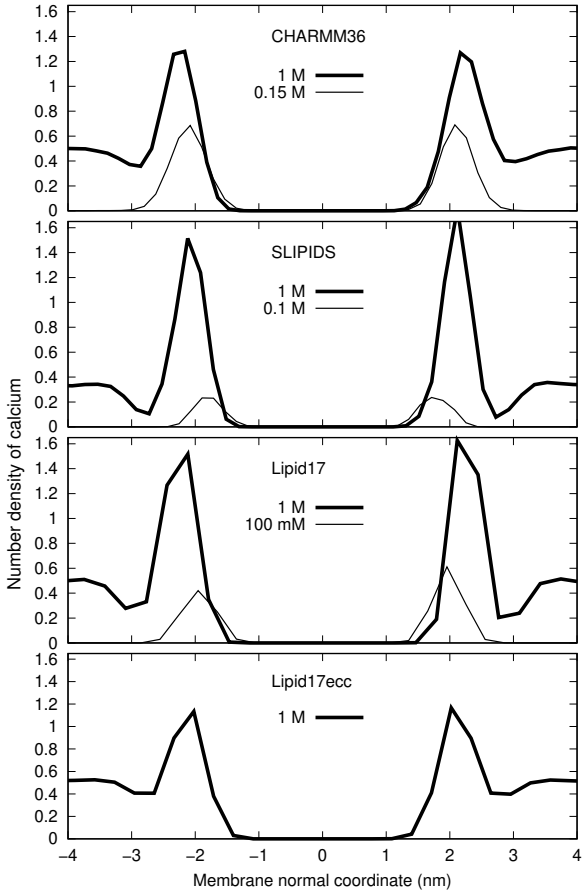

FIG. 10: Calcium ion density profiles along membrane normal from simulations of POPC:POPG (1:1) mixtures with different force fields.

CONCLUSIONS

AP is grateful to the Centro de Supercomputacin de Galicia (CESGA) for use of the Finis Terrae computer

* samuli.ollila@helsinki.fi

[1] C. Sohlenkamp and O. Geiger, FEMS Microbiology Reviews **40**, 133 (2015).

[2] J. E. Vance, Traffic **16**, 1 (2015).

[3] E. Calzada, O. Onguka, and S. M. Claypool (Academic Press, 2016), vol. 321 of *International Review of Cell and Molecular Biology*, pp. 29 – 88.

[4] D. Patel and S. N. Witt, Oxidative Medicine and Cellular Longevity **2017**, 4829180 (2017).

[5] S. Furse, Journal of Chemical Biology **10**, 1 (2017).

[6] P. Hariharan, E. Tikhonova, J. Medeiros-Silva, A. Jeucken, M. V. Bogdanov, W. Dowhan, J. F. Brouwers, M. Weingarth, and L. Guan, BMC Biology **16**, 85 (2018).

[7] P. L. Yeagle, Biochimica et Biophysica Acta (BBA) - Biomembranes **1838**, 1548 (2014), membrane Structure and Function: Relevance in the Cell's Physiology, Pathology and Therapy.

[8] L. V. Chernomordik and M. M. Kozlov, Nature Struct. Mol. Biol. **15**, 675 (2008).

[9] H. U. Gally, G. Pluschke, P. Overath, and J. Seelig, Biochemistry **20**, 1826 (1981).

[10] P. Scherer and J. Seelig, EMBO J. **6** (1987).

[11] J. Seelig, Cell Biology International Reports **14**, 353 (1990), ISSN 0309-1651, URL http://www.sciencedirect.com/science/article/pii/030916519091204H.

[12] R. Wohlgemuth, N. Waespe-Sarcevic, and J. Seelig, Biochemistry **19**, 3315 (1980).

[13] G. Büldt and R. Wohlgemuth, The Journal of Membrane Biology **58**, 81 (1981), ISSN 1432-1424, URL http://dx.doi.org/10.1007/BF01870972.

[14] J. Seelig, Q. Rev. Biophys. **10**, 353 (1977).

[15] J. H. Davis, Biochim. Biophys. Acta **737**, 117 (1983).

[16] D. J. Semchyschyn and P. M. Macdonald, Magn. Res. Chem. **42**, 89 (2004).

[17] A. Botan, F. Favela-Rosales, P. F. J. Fuchs, M. Javanainen, M. Kanduč, W. Kulig, A. Lamberg, C. Loison, A. Lyubartsev, M. S. Miettinen, et al., J. Phys. Chem. B **119**, 15075 (2015).

[18] H. S. Antila, P. Buslaev, F. Favela-Rosales, T. Mendes Ferreira, I. Gushchin, M. Javanainen, B. Kav, J. J. Madsen, J. Melcr, M. S. Miettinen, et al., The Journal of Physical Chemistry B p. acs.jpcb.9b06091 (2019), ISSN 1520-6106.

[19] A. H. de Vries, A. E. Mark, and S. J. Marrink, The Journal of Physical Chemistry B **108**, 2454 (2004).

[20] K. Murzyn, T. Rg, and M. Pasenkiewicz-Gierula, Biophysical Journal **88**, 1091 (2005), ISSN 0006-3495, URL http://www.sciencedirect.com/science/article/pii/S0006349505731799.

[21] U. R. Pedersen, C. Leidy, P. Westh, and G. H. Peters, Biochimica et Biophysica Acta (BBA) - Biomembranes **1758**, 573 (2006).

[22] W. Zhao, T. Rg, A. A. Gurtovenko, I. Vattulainen, and M. Karttunen, Biophysical Journal **92**, 1114 (2007), ISSN 0006-3495, URL http://www.sciencedirect.com/science/article/pii/S0006349507709232.

[23] A. A. Gurtovenko and I. Vattulainen, J. Phys. Chem. B **112**, 1953 (2008).

[24] W. Zhao, T. Rg, A. A. Gurtovenko, I. Vattulainen, and M. Karttunen, Biochimie **90**, 930 (2008), ISSN 0300-9084, URL http://www.sciencedirect.com/science/article/pii/S0300908408000692.

[25] J. Hnin, W. Shinoda, and M. L. Klein, The Journal of Physical Chemistry B **113**, 6958 (2009).

[26] A. Kukol, J. Chem. Theory Comput. **5**, 615 (2009).

[27] H.-H. G. Tsai, W.-X. Lai, H.-D. Lin, J.-B. Lee, W.-F. Juang, and W.-H. Tseng, Biochimica et Biophysica Acta (BBA) - Biomembranes **1818**, 2742 (2012), ISSN 0005-2736, URL http://www.sciencedirect.com/science/article/pii/S0005273612001873.

[28] C. J. Dickson, L. Rosso, R. M. Betz, R. C. Walker, and I. R. Gould, Soft Matter **8**, 9617 (2012).

[29] R. M. Venable, Y. Luo, K. Gawrisch, B. Roux, and R. W. Pastor, The Journal of Physical Chemistry B **117**, 10183 (2013).

[30] C. J. Dickson, B. D. Madej, A. A. Skjevik, R. M. Betz, K. Teigen, I. R. Gould, and R. C. Walker, J. Chem. Theory Comput. **10**, 865 (2014).

[31] N. A. Berglund, T. J. Piggot, D. Jefferies, R. B. Sessions, P. J. Bond, and S. Khalid, PLOS Computational Biology **11**, 1 (2015), URL https://doi.org/10.1371/journal.pcbi.1004180.

[32] G. Cevc, Biochim. Biophys. Acta - Rev. Biomemb. **1031**, 311 (1990).

[33] J.-F. Tocanne and J. Teissié, Biochim. Biophys. Acta - Reviews on Biomembranes **1031**, 111 (1990).

[34] M. Roux and M. Bloom, Biochemistry **29**, 7077 (1990).

[35] A. Catte, M. Girych, M. Javanainen, C. Loison, J. Melcr, M. S. Miettinen, L. Monticelli, J. Maatta, V. S. Oganesyan, O. H. S. Ollila, et al., Phys. Chem. Chem. Phys. **18**, 32560 (2016).

[36] J. Marra and J. Israelachvili, Biochemistry **24**, 4608 (1985).

[37] H. Hauser and G. Shipley, Biochimica et Biophysica Acta (BBA) - Biomembranes **813**, 343 (1985), ISSN 0005-2736, URL http://www.sciencedirect.com/science/article/pii/0005273685902512.

[38] G. W. Feigenson, Biochemistry **25**, 5819 (1986).

[39] M. Roux and M. Bloom, Biophys. J. **60**, 38 (1991).

[40] J. Melcr, H. Martinez-Seara, R. Nencini, J. Kolafa, P. Jungwirth, and O. H. S. Ollila, The Journal of Physical Chemistry B **122**, 4546 (2018).

[41] J. Melcr, T. Ferreira, P. Jungwirth, and O. H. S. Ollila, *Improved cation binding to lipid bilayer with negatively charged pops by effective inclusion of electronic polarization*, submitted, URL https://github.com/ohsOllila/ecc_lipids/blob/master/Manuscript/manuscript.pdf.

[42] S. V. Dvinskikh, H. Zimmermann, A. Maliniak, and D. Sandstrom, J. Magn. Reson. **168**, 194 (2004).

[43] J. D. Gross, D. E. Warschawski, and R. G. Griffin, J. Am. Chem. Soc. **119**, 796 (1997).

[44] T. M. Ferreira, F. Coreta-Gomes, O. H. S. Ollila, M. J. Moreno, W. L. C. Vaz, and D. Topgaard, Phys. Chem. Chem. Phys. **15**, 1976 (2013).

[45] T. M. Ferreira, R. Sood, R. Bärenwald, G. Carlström, D. Topgaard, K. Saalwächter, P. K. J. Kinnunen, and O. H. S. Ollila, Langmuir **32**, 6524 (2016).

[46] D. Marsh, *Handbook of Lipid Bilayers, Second Edition* (RSC press, 2013).

[47] N. Michaud-Agrawal, E. J. Denning, T. B. Woolf, and O. Beckstein, Journal of Computational Chemistry **32**, 2319 (2011), https://onlinelibrary.wiley.com/doi/pdf/10.1002/jcc.21787,

URL https://onlinelibrary.wiley.com/doi/abs/10.1002/jcc.21787.

[48] Richard J. Gowers, Max Linke, Jonathan Barnoud, Tyler J. E. Reddy, Manuel N. Melo, Sean L. Seyler, Jan Domaski, David L. Dotson, Sbastien Buchoux, Ian M. Kenney, et al., in *Proceedings of the 15th Python in Science Conference*, edited by Sebastian Benthall and Scott Rostrup (2016), pp. 98 – 105.

[49] ohsOllila and et al., *Match github repository*, URL https://github.com/NMRLipids/MATCH.

[50] P. Fuchs and et al., *Buildh github repository*, URL https://github.com/patrickfuchs/buildH.

[51] T. J. Piggot, J. R. Allison, R. B. Sessions, and J. W. Essex, J. Chem. Theory Comput. **13**, 5683 (2017).

[52] M. Abraham, D. van der Spoel, E. Lindahl, B. Hess, and the GROMACS development team, *GROMACS user manual version 5.0.7* (2015), URL www.gromacs.org.

[53] M. Javanainen, *Simulation of a POPE bilayer at 310K with the CHARMM36 force field* (2019), URL https://doi.org/10.5281/zenodo.2641987.

[54] PEON, *CHARMM36 POPE Bilayer Simulation (Last 100 ns, 310 K)* (2019), URL https://doi.org/10.5281/zenodo.3237461.

[55] A. PEN, *CHARMM36 POPE Bilayer Simulation (Last 100 ns, 150 mM NaCl, 310 K)* (2019), URL https://doi.org/10.5281/zenodo.2577454.

[56] T. Piggot, *CHARMM36-UA POPE Simulations (versions 1 and 2) 310 K (NOTE: hexagonal membrane and POPE is called PEUA)* (2018), URL https://doi.org/10.5281/zenodo.1293774.

[57] J. P. M. Jämbeck and A. P. Lyubartsev, J. Chem. Theory Comput. **8**, 2938 (2012).

[58] F. Favela-Rosales, *MD simulation trajectory of a fully hydrated DPPE bilayer: SLIPIDS, Gromacs 5.0.4. 2017.* (2017), URL https://doi.org/10.5281/zenodo.495247.

[59] T. Piggot, *Slipids POPE Simulations (versions 1 and 2) 310 K (NOTE: hexagonal membrane)* (2018), URL https://doi.org/10.5281/zenodo.1293813.

[60] A. Peon, *SLIPID POPE Bilayer Simulation (Last 100 ns, 310 K)* (2019), URL https://doi.org/10.5281/zenodo.3231342.

[61] A. PEN, *SLIPID POPE Bilayer Simulation (Last 100 ns, 150 mM NaCl, 310 K)* (2019), URL https://doi.org/10.5281/zenodo.2578069.

[62] T. Piggot, *GROMOS-CKP DPPE Simulations (versions 1 and 2) 342 K* (2018), URL https://doi.org/10.5281/zenodo.1293957.

[63] T. Piggot, *GROMOS-CKP POPE Simulations (versions 1 and 2) 313 K* (2018), URL https://doi.org/10.5281/zenodo.1293932.

[64] A. PEON, *GROMOS POPE Bilayer Simulation (Last 100 ns, 310 K)* (2019), URL https://doi.org/10.5281/zenodo.3237754.

[65] A. PEN, *Gromos POPE Bilayer Simulation (Last 100 ns, 150 mM NaCl, 310 K)* (2019), URL https://doi.org/10.5281/zenodo.2574491.

[66] T. Piggot, *GROMOS-CKP DOPE Simulations (versions 1 and 2) 271 K* (2018), URL https://doi.org/10.5281/zenodo.1293941.

[67] T. Piggot, *GROMOS 43A1-S3 POPE Simulations (versions 1 and 2) 313 K (NOTE: anisotropic pressure coupling)* (2018), URL https://doi.org/10.5281/zenodo.1293762.

[68] T. Piggot, *OPLS-UA POPE Simulations (versions 1 and 2) 303 K with vdW on H atoms* (2018), URL https://doi.org/10.5281/zenodo.1293853.

[69] T. Piggot, *Opls-ua pope simulations (versions 1 and 2) 303 k* (2018), URL https://doi.org/10.5281/zenodo.1293855.

[70] T. Rg, A. Orowski, A. Llorente, T. Skotland, T. Sylvnne, D. Kauhanen, K. Ekroos, K. Sandvig, and I. Vattulainen, Data in Brief **7**, 1171 (2016), ISSN 2352-3409, URL http://www.sciencedirect.com/science/article/pii/S2352340916301755.

[71] M. Javanainen, *Simulation of a POPE bilayer, lipid model based on OPLS-aa by Rog et al.* (2019), URL https://doi.org/10.5281/zenodo.3571071.

[72] T. Piggot, *Berger POPE Simulations (versions 1 and 2) 303 K - de Vries repulsive H* (2018), URL https://doi.org/10.5281/zenodo.1293889.

[73] T. Piggot, *Berger POPE Simulations (versions 1 and 2) 303 K - larger repulsive H* (2018), URL https://doi.org/10.5281/zenodo.1293891.

[74] T. Piggot, *Berger DOPE Simulations (versions 1 and 2) 271 K - de Vries repulsive H* (2018), URL https://doi.org/10.5281/zenodo.1293928.

[75] T. Piggot, *Berger DOPE Simulations (versions 1 and 2) 271 K - larger repulsive H* (2018), URL https://doi.org/10.5281/zenodo.1293905.

[76] A. PEON, *LIPID17 POPE Bilayer Simulation (Last 100 ns, 310 K)* (2019), URL https://doi.org/10.5281/zenodo.3378970.

[77] A. PEN, *LIPID17 POPE Bilayer Simulation (Last 100 ns, 150 mM NaCl, 310 K)* (2019), URL https://doi.org/10.5281/zenodo.2577305.

[78] O. H. S. Ollila, *POPG lipid bilayer simulation at T298K ran with MODEL_CHARMM_GUI force field and Gromacs* (2017), URL https://doi.org/10.5281/zenodo.1011096.

[79] A. PEN, *CHARMM36 POPG Bilayer Simulation (Last 100 ns, 150 mM NaCl, 310 K)* (2019), URL https://doi.org/10.5281/zenodo.2573531.

[80] ANTONIO, *CHARMM36 POPG Bilayer Simulation (Last 100 ns, 310 K)* (2019), URL https://doi.org/10.5281/zenodo.3237463.

[81] J. P. M. Jämbeck and A. P. Lyubartsev, Phys. Chem. Chem. Phys. **15**, 4677 (2013).

[82] F. Favela-Rosales, *MD simulation trajectory of a fully hydrated POPG bilayer: SLIPIDS, Gromacs 5.0.4. 2017.* (2017), URL https://doi.org/10.5281/zenodo.546133.

[83] F. Favela-Rosales, *MD simulation trajectory of a fully hydrated DPPG bilayer @314K: SLIPIDS, Gromacs 5.0.4. 2017.* (2017), URL https://doi.org/10.5281/zenodo.546136.

[84] F. Favela-Rosales, *MD simulation trajectory of a fully hydrated DPPG bilayer @298K: SLIPIDS, Gromacs 5.0.4. 2017.* (2017), URL https://doi.org/10.5281/zenodo.546135.

[85] A. PEN, *SLIPID POPG Bilayer Simulation (Last 100 ns, 310 K)* (2019), URL https://doi.org/10.5281/zenodo.3364460.

[86] A. PEN, *SLIPID POPG Bilayer Simulation (Last 100 ns, 150 mM NaCl, 310 K)* (2019), URL https://doi.org/10.5281/zenodo.2633773.

[87] A. PEON, *LIPID17 POPG Bilayer Simulation (Last 100 ns, 310 K)* (2019), URL https://doi.org/10.5281/zenodo.3247659.

[88] A. PEN, *LIPID17 POPG Bilayer Simulation (Last 100 ns, 150 mM NaCl, 310 K)* (2019), URL https://doi.org/10.

5281/zenodo.2573905.
[89] A. PEON, *GROMOS POPG Bilayer Simulation (Last 100 ns, 310 K)* (2019), URL https://doi.org/10.5281/zenodo.3266166.
[90] A. PEN, *Gromos POPG Bilayer Simulation (Last 100 ns, 150 mM NaCl, 310 K)* (2019), URL https://doi.org/10.5281/zenodo.3257649.
[91] A. Pen, *CHARMM36 POPC Bilayer Simulation (Last 100 ns, 150 mM NaCl, 310 K)* (2019), URL https://doi.org/10.5281/zenodo.2628335.
[92] A. PEN, *CHARMM36 POPC-POPG 7:3 Bilayer Simulation (Last 100 ns, 150 mM NaCl, 310 K)* (2019), URL https://doi.org/10.5281/zenodo.2580902.
[93] J. J. Madsen, *MD simulations of bilayers containing PC/PG mixtures and CaCl_2: 250POPC_250POPG_neutral* (2019), URL https://doi.org/10.5281/zenodo.3483787.
[94] J. J. Madsen, *MD simulations of bilayers containing PC/PG mixtures and CaCl_2: 250POPC_250POPG_0.15MCaCl_2* (2019), URL https://doi.org/10.5281/zenodo.3483789.
[95] J. J. Madsen, *MD simulations of bilayers containing PC/PG mixtures and CaCl_2: 250POPC_250POPG_1MCaCl_2* (2019), URL https://doi.org/10.5281/zenodo.3483793.
[96] J. J. Madsen, *MD simulations of bilayers containing PC/PG mixtures and CaCl_2: 400POPC_100POPG_neutral* (2019), URL https://doi.org/10.5281/zenodo.3483783.
[97] J. J. Madsen, *MD simulations of bilayers containing PC/PG mixtures and CaCl_2: 400POPC_100POPG_1MCaCl_2* (2019), URL https://doi.org/10.5281/zenodo.3483785.
[98] C. Papadopoulos and P. F. Fuchs, *CHARMM36 pure POPC MD simulation (300 K - 300ns - 1 bar)* (2018), URL https://doi.org/10.5281/zenodo.1306800.
[99] C. Papadopoulos and P. F. Fuchs, *CHARMM36 POPC/POPE (50%-50%) MD simulation (300 K - 300ns - 1 bar)* (2018), URL https://doi.org/10.5281/zenodo.1306821.
[100] A. PEN, *SLIPID POPC Bilayer Simulation (Last 100 ns, 150 mM NaCl, 310 K)* (2019), URL https://doi.org/10.5281/zenodo.2574689.
[101] A. PeON, *SLIPID POPC-POPG 7:3 Bilayer Simulation (Last 100 ns, 310 K)* (2019), URL https://doi.org/10.5281/zenodo.3240156.
[102] M. Javanainen, *Simulations of POPC:POPG 1:1 membranes with varying levels of CaCl_2 using the Slipids force field* (2020), URL https://doi.org/10.5281/zenodo.3613573.
[103] S. Virtanen, *LIPID17 POPC-POPG 50:50 MD simulation, Na+ counterions, 298K* (2019), URL https://doi.org/10.5281/zenodo.3520479.
[104] B. Amlie and F. P. F.J., *Berger pure POPC MD simulation (300 K - 300ns - 1 bar)* (2018), URL https://doi.org/10.5281/zenodo.1402417.
[105] B. Amlie and F. P. F.J., *Berger POPC/POPE (50:50 ratio) MD simulation (300 K - 400ns - 1 bar)* (2018), URL https://doi.org/10.5281/zenodo.1402449.
[106] B. Amlie and F. P. F.J., *Berger POPC/DOPE (50:50 ratio) MD simulation (300 K - 300ns - 1 bar)* (2018), URL https://doi.org/10.5281/zenodo.1402441.
[107] B. Amlie and F. P. F.J., *Berger pure DOPC MD simulation (300 K - 300ns - 1 bar)* (2018), URL https://doi.org/10.5281/zenodo.1402411.
[108] B. Amlie and F. P. F.J., *Berger DOPC/DOPE (50:50 ratio) MD simulation (300 K - 300ns - 1 bar)* (2018), URL https://doi.org/10.5281/zenodo.1402437.
[109] J. Seelig and H. U. Gally, Biochemistry **15**, 5199 (1976).
[110] F. Borle and J. Seelig, Chemistry and Physics of Lipids **36**, 263 (1985).
[111] O. S. Ollila and G. Pabst, Biochimica et Biophysica Acta (BBA) - Biomembranes **1858**, 2512 (2016).
[112] J. L. Browning and J. Seelig, Biochemistry **19**, 1262 (1980).
[113] P. Mukhopadhyay, L. Monticelli, and D. P. Tieleman, Biophysical Journal **86**, 1601 (2004).
[114] M. Dahlberg, A. Marini, B. Mennucci, and A. Maliniak, The Journal of Physical Chemistry A **114**, 4375 (2010).
[115] P. M. Macdonald and J. Seelig, Biochemistry **26**, 1231 (1987).
[116] J. Seelig, P. M. MacDonald, and P. G. Scherer, Biochemistry **26**, 7535 (1987).
[117] H. S. Antila, P. Buslaev, F. Favela-Rosales, T. Mendes Ferreira, I. Gushchin, M. Javanainen, B. Kav, J. J. Madsen, J. Melcr, M. S. Miettinen, et al., The Journal of Physical Chemistry B **0**, null (0), https://doi.org/10.1021/acs.jpcb.9b06091, URL https://doi.org/10.1021/acs.jpcb.9b06091.
[118] C. Par and M. Lafleur, Biophysical Journal **74**, 899 (1998), ISSN 0006-3495, URL http://www.sciencedirect.com/science/article/pii/S0006349598740135.
[119] J. Pan, F. A. Heberle, S. Tristram-Nagle, M. Szymanski, M. Koepfinger, J. Katsaras, and N. Kuerka, Biochimica et Biophysica Acta (BBA) - Biomembranes **1818**, 2135 (2012).
[120] H. Akutsu and J. Seelig, Biochemistry **20**, 7366 (1981).

ToDo